Second law analysis of heat transfer in swirling flow of Bingham fluid by a rotating disk subjected to suction effect

Meraj Mustafa [a, 1], Maria Tabassum [a] and Mahmood Rahi [b]

[a] *School of Natural Sciences (SNS), National University of Sciences and Technology (NUST), Islamabad 44000, Pakistan*

[b] *Higher Colleges of Technology (HCT), Abu Dhabi 5464, United Arab Emirates (UAE)*

Abstract: This framework presents heat transfer analysis for swirling flow of viscoplastic fluid bounded by a permeable rotating disk. Problem formulation is made through constitutive relations of Bingham fluid model. Viscous dissipation effects are preserved in the mathematical model. Entropy production analysis is made which is yet to be explored for the von-Kármán flow of non-Newtonian fluids. Having found the similarity equations, these have been dealt numerically for broad parameter values. The solutions are remarkably influenced by wall suction parameter (A) and Bingham number (Bn) which measures the fluid yield stress. Akin to earlier numerical results, thermal boundary layer suppresses upon increasing wall suction velocity. Thermal penetration depth is much enhanced when fluid yield stress becomes large. Higher heat transfer rate can be accomplished by employing higher suction velocity at the disk. However, deterioration in heat transfer is anticipated as fluid yield stress enlarges. Current numerical results are in perfect line with those of an existing article in limiting sense.

Keywords: Bingham fluid; Rotating disk; Viscoplastic fluid; Entropy generation; Convection

1. Introduction

The steady-state laminar flow induced by a disk of large radius rotating with constant angular velocity about the vertical axis is a classical fluid dynamics problem that has both theoretical and practical significance. von-Kármán [1] showed that such problem exhibits exact solution of three-dimensional Navier-Stokes equations. Within the boundary layer, there is insufficient radial pressure gradient to overcome centrifugal effect. The result is a radially outward fluid motion near the disk, and for the reasons of continuity, such motion is compensated by axial flow directed back towards the disk. Cochran [2] found accurate solutions of von-Kármán problem by numerical integration of governing equations. Bachelor [3] noticed that von-Kármán flow is just a limiting case of the problem in which both disk and fluid at infinity are in a state of rotation about the same axis. Another limiting case where infinite plane is stationary and fluid high above that plane rotates with uniform angular velocity was firstly discovered by Bödewadt [4]. Ackroyd [5] studied mass transfer to swirling flow along a permeable rotating disk. He provided an accurate series solution comprising pure exponential functions with negative exponents. Heat transfer to laminar flow by heated rotating disk with radially varying surface temperature was addressed by Millsaps and Pohlhausen [6]. After these initial contributions, a vast wealth of literature was subsequently published addressing rotating disk induced flows under different

[1] Corresponding author Tel.: + 92 51 90855596
E-mail address: meraj_mm@hotmail.com (M. Mustafa)

physical situations such as wall permeability, transverse magnetic field, non-Newtonian effects and different wall conditions (see [7]- [16] and refs. there in.).

There has been increasing recognition of the fact that most fluids of practical and industrial interest do not conform to the Newtonian flow behavior and are accordingly known as non-Newtonian fluids. Commonly encountered food items (flavored milk, butter, jellies, mayonnaise, yoghurt, whipped cream, ketchup etc.), pharmaceutical products (suspension, gels, multiphase mixtures etc.), biological fluids (blood, synovial fluid, saliva, semen etc.), polymeric liquids, lubricants, paints and greases show non-Newtonian behavior. Among various classes of non-Newtonian materials are those exhibiting viscoplastic properties due to their ability to deform only if the shear stress reaches a certain minimum value called yield stress. Waxy crude oils, paints, jellies, emulsions, pastes and foams are common viscoplastic materials. Bingham fluid model is perhaps the simplest possible representation of the viscoplastic behavior. Furthermore, heat transfer phenomenon is associated with fluid flows in wide spectrum of engineering and geophysical applications. Heat transfer plays enormous role in many industrial sectors such as in energy production, in automotive industry, in chemical and food processing industries, in home appliances and in aerospace engineering. Despite the aforementioned applications, modest attention is paid towards the treatment of von-Kármán flow problem with non-Newtonian or heat transfer effects. Andersson et al. [17] computed accurate numerical results for von-Kármán flow of power-law fluids for broad range of power-law index. They remarked that accuracy of numerical results deteriorates with increasing deviation of flow behavior index from unity. von Kármán flow of Bingham fluid was firstly addressed by Ahmadpour and Sadeghy [18]. They showed that the problem admits similarity solutions even in case of Bingham fluids. Their results demonstrate remarkable effects of fluid yield stress on the velocity components. Similar problem was re-investigated in a later paper by Guha and Sengupta [19] with a focus on different computational approaches. Griffiths [20] analyzed the flow of shear-thinning/thickening fluids along an infinite disk in rotating frame of reference utilizing different fluid models. Heat transfer to von Kármán flow of power-law fluid was considered by Ming et al. [21] through a generalized Fourier model based on temperature dependent thermal conductivity. Xun et al. [22] analyzed the flow of shear-thinning fluid along a variable thickness rotating disk. Very recently, Tabassum and Mustafa [23] examined the von-Kármán flow of Reiner-Rivlin fluid subject to partial slip using shooting method.

Prime motive of this research is to formulate and resolve heat transfer problem for von-Kármán flow of Bingham fluid considering isothermal wall condition. Hence the flow analysis of Ahmadpour and Sadeghy [18] is extended for heat transfer effects with viscous dissipation and wall suction aspects. Finally, entropy generation analysis is made through second law of thermodynamics. In the next section, we present similar form of governing equations using von-Kármán transformations. The effects of fluid yield stress and wall suction on velocity, temperature and entropy generation are explained graphically in section 3. Finally, the important points are highlighted in the final section.

2. Problem Formulation

Suppose a permeable disk of large radius R lying in the plane $z = 0$ rotates with constant angular velocity in an otherwise stationary viscoplastic fluid obeying Bingham fluid model. It is obvious to perform mathematical formulation in cylindrical coordinate system (r, ϕ, z). All three velocities (u, v, w) will be non-zero and, owing to the rotational symmetry, these will not change by varying azimuthal coordinate ϕ. The temperature at the disk is assumed constant at T_w while T_∞ denotes fluid temperature high above the surface. Heat generation due to fluid friction will be factored in the analysis. Relevant equations describing fluid motion and heat transfer above a rotating disk can be cast into the following forms [18]:

$$\frac{\partial u}{\partial r}+\frac{u}{r}+\frac{\partial w}{\partial z}=0, \tag{1}$$

$$\rho\left(u\frac{\partial u}{\partial r}+w\frac{\partial u}{\partial z}-\frac{v^2}{r}\right)=-\frac{\partial p}{\partial r}+\frac{\partial \tau_{rr}}{\partial r}+\frac{\partial \tau_{rz}}{\partial z}+\frac{\tau_{rr}-\tau_{\phi\phi}}{r}, \tag{2}$$

$$\rho\left(u\frac{\partial v}{\partial r}+w\frac{\partial v}{\partial z}+\frac{uv}{r}\right)=\frac{1}{r^2}\frac{\partial}{\partial r}\left(r^2\tau_{r\phi}\right)+\frac{\partial \tau_{z\phi}}{\partial z}+\frac{\tau_{r\phi}-\tau_{\phi r}}{r}, \tag{3}$$

$$\rho\left(u\frac{\partial w}{\partial r}+w\frac{\partial w}{\partial z}\right)=-\frac{\partial p}{\partial z}+\frac{1}{r}\frac{\partial}{\partial r}(r\tau_{rz})+\frac{\partial \tau_{zz}}{\partial z}, \tag{4}$$

Considering no-slip and permeability at the disk, one has:

$$u=0,\ \ v=r\omega,\ \ w=-w_0\ \text{ at } z=0, \tag{5}$$

and since lateral velocities become zero outside the boundary layer, we have:

$$u\to 0,\ \ v\to 0 \text{ as } z\to\infty. \tag{6}$$

Now Cauchy stress tensor for Bingham fluid is given by:

$$\begin{cases}\tau_{ij}=\left(\dfrac{\tau_y}{\dot{\gamma}}+\mu_p\right)e_{ij}\equiv\eta(\dot{\gamma})e_{ij} & \text{for } \tau\ge\tau_y,\\ \quad =0 & \text{for } \tau<\tau_y,\end{cases} \tag{7}$$

where $\dot{\gamma}=(1/2\, e_{ij}e_{ji})^{1/2}$ is the second invariant of the deformation rate tensor in which $e_{ij}=(\partial u_i/\partial x_j+\partial u_j/\partial x_i)$ are components of the deformation rate tensor, τ_y is the fluid yield stress, μ_p is the plastic viscosity and $\eta(\dot{\gamma})$ denotes the apparent viscosity.

Through Eq. (7), the components of stress tensor τ are obtained as follows:

$$\begin{gathered}\tau_{rr}=\eta\left(2\frac{\partial u}{\partial r}\right);\ \tau_{\phi\phi}=\eta\left(2\frac{u}{r}\right);\ \tau_{zz}=\eta\left(2\frac{\partial w}{\partial z}\right);\\ \tau_{r\phi}=\eta\left\{r\frac{\partial}{\partial r}\left(\frac{v}{r}\right)\right\};\ \tau_{\phi z}=\eta\left(\frac{\partial v}{\partial z}\right);\ \tau_{rz}=\eta\left(\frac{\partial u}{\partial z}+\frac{\partial w}{\partial r}\right),\end{gathered} \tag{8}$$

in which the apparent viscosity η has the following form:

$$\eta(r,z)=\mu_p+\frac{\tau_y}{\sqrt{2\left(\frac{\partial u}{\partial r}\right)^2+2\left(\frac{u}{r}\right)^2+2\left(\frac{\partial w}{\partial z}\right)^2+\left[r\frac{\partial}{\partial r}\left(\frac{v}{r}\right)\right]^2+\left(\frac{\partial v}{\partial z}\right)^2+\left(\frac{\partial u}{\partial z}+\frac{\partial w}{\partial r}\right)^2}}, \tag{9}$$

By making use of von-Kármán transformations:

$$\begin{gathered}\zeta=\frac{z}{\sqrt{\nu_p/\omega}},\\ (u,v,w)=\left(r\omega F(\zeta),r\omega G(\zeta),H(\zeta)\sqrt{\nu_p\omega},\right),\\ (p,T)=\left(p_\infty-\omega\mu P(\zeta),T_\infty+(T_w-T_\infty)\theta(\zeta)\right),\end{gathered} \tag{10}$$

where ζ is the dimensionless distance measured along the rotation axis, the governing equations transform into the following locally similar equations (see ref. [18] for details):

$$2F + H' = 0, \tag{11}$$

$$F^2 - G^2 + HF' = \left(1 + \frac{Bn}{\wedge}\right)F'' - \frac{2Bn}{\wedge^3}F(G'^2 + F'^2) - \frac{Bn}{2\wedge^3}F'\left[8FF' + 4H'H'' + 2r^{\star 2}Re(G'G'' + F'F'')\right], \tag{12}$$

$$2FG + HG' = \left(1 + \frac{Bn}{\wedge}\right)G'' - \frac{Bn}{2\wedge^3}G'\left[8FF' + 4H'H'' + 2r^{\star 2}Re(G'G'' + F'F'')\right], \tag{13}$$

where $\wedge \equiv \sqrt{4F^2 + 2H'^2 + Re[r^{\star 2}(G'^2 + F'^2)]}$.

The transformed conditions are given below:

$$F(0) = 0, \;\; G(0) = 1, \;\; H(0) = -A \;\text{ at } \zeta = 0, \tag{14}$$

$$F \to 0, \;\; G \to 0 \;\text{ as } \zeta \to \infty. \tag{15}$$

In Eqs. (12)-(15), $A = w_0/\sqrt{\nu w}$ is the wall suction parameter, $r^\star = r/R$ stands for non-dimensional radius, $Bn = \tau_y/\mu_p\omega$ is the Bingham number and $Re = R^2\omega/\nu_p$ represents the Reynolds number for disk of radius R. In a recent paper by Rahman and Andersson [27], it was shown that upward axial flow produces unphysical temperature profiles for Bödewadt flow. Such tendency is likely to occur when injection is introduced in the von- Kármán's problem. Hence present paper focuses only on suction ($A > 0$).

2.1. Heat transfer analysis

Heat transfer takes place as a result of difference in temperature at the disk surface and that of the ambient fluid. In presence of viscous dissipation, the energy equation is given by:

$$\rho c_p\left(u\frac{\partial T}{\partial r} + w\frac{\partial T}{\partial z}\right) = k\left(\frac{1}{r}\frac{\partial T}{\partial r} + \frac{\partial^2 T}{\partial r^2} + \frac{\partial^2 T}{\partial z^2}\right) + \Phi, \tag{16}$$

where k stands for thermal conductivity, c_p for specific heat capacity and Φ represents the viscous dissipation term given below:

$$\Phi = \tau_{rr}\left(\frac{\partial u}{\partial r}\right) + \tau_{\phi\phi}\left(\frac{u}{r}\right) + \tau_{zz}\left(\frac{\partial w}{\partial z}\right) + \tau_{r\phi}\left[r\frac{\partial}{\partial r}\left(\frac{v}{r}\right)\right] + \tau_{rz}\left(\frac{\partial u}{\partial z} + \frac{\partial w}{\partial r}\right) + \tau_{\phi z}\left(\frac{\partial v}{\partial z}\right). \tag{17}$$

By using $\theta(\zeta) = (T - T_\infty)/(T_w - T_\infty)$ together with the von-Kármán transformations, equation (16) becomes,

$$\frac{1}{Pr}\theta'' - H\theta' + \frac{Ec}{Re}(\wedge + Bn)\wedge = 0, \tag{18}$$

in which $Pr = \mu c_p/k$ denotes the Prandtl number and $Ec = R^2\omega^2/C_p\Delta T$ is the Eckert number. Eq. (18) is to be solved subject to the conditions:

$$\theta(0) = 1 \;\text{ and }\; \theta(\infty) = 0. \tag{19}$$

2.2. Skin friction coefficient, Nusselt number and volumetric flow rate

Skin friction coefficient C_f measuring the drag coefficient at the surface is defined below:

$$C_f = \frac{\sqrt{\tau_r^2 + \tau_\phi^2}}{\rho(r\omega)^2}, \tag{20}$$

where τ_r and τ_ϕ denote the radial and azimuthal wall stresses respectively which can be evaluated from Eq. (8). Eq. (21) in view of transformations (10) becomes:

$$r^* C_f = \frac{Bn}{Re} + \left\{\frac{(F'(0))^2 + \left(G'(0)\right)^2}{Re}\right\}^{1/2}. \tag{21}$$

Nusselt number Nu measuring the importance of convective heat transfer relative to conductive heat transfer is defined as follows:

$$Nu = \frac{Lq_w}{k(T_w - T_\infty)}, \tag{23}$$

where q_w denotes the wall heat flux. Using the length scale L as $\sqrt{\nu_p/\omega}$, Eq. (23) reduces to:

$$Nu = -\theta'(0). \tag{24}$$

The pumping efficiency of the disk can be computed using the following definite integral [13];

$$Q = \int_0^R -w(\infty)2\pi r dr = -H(\infty)\pi\sqrt{\nu\omega}\, R^2. \tag{25}$$

2.3. Entropy generation equation

The entropy generation rate is defined as follows (see Rashidi et al. [24], Sheremet et al. [25], Hayat et al. [26] etc.):

$$\dot{S}'''_{\text{gen}} = \frac{k}{T_\infty^2}\left[\left(\frac{\partial T}{\partial r}\right)^2 + \left(\frac{1}{r}\frac{\partial T}{\partial \theta}\right)^2 + \left(\frac{\partial T}{\partial z}\right)^2\right] + \frac{\Phi}{T_\infty}, \tag{26}$$

First part of Eq. (26) signifies the entropy production due to thermal irreversibility and second part corresponds to the fluid friction irreversibility.

The dimensionless form of the entropy generation rate is the entropy generation number N_G which is the ratio of the actual entropy generation rate $\dot{S}'''_{\text{gen}}$ to the characteristic entropy generation rate $\dot{S}_0 = (k\omega\Delta T/\nu T_\infty)$. It is evaluated as follows:

$$N_G = \dot{S}'''_{\text{gen}}/(k\omega\Delta T/\nu T_\infty) = \alpha\theta'^2 + \frac{Pr.Ec}{Re}(\wedge + Bn)\wedge, \tag{27}$$

where $\alpha = \Delta T/T_\infty$ measures the wall and ambient temperature difference. To determine the contribution of entropy generation due to heat transfer, we introduce Bejan number Be as follows:

$$Be = \frac{\text{Entropy generation due to heat transfer}}{\text{Entropy generation number}}, \tag{28}$$

$$Be = \frac{\alpha\theta'^2}{\alpha\theta'^2 + \frac{PrEc}{Re}(\wedge + Bn)\wedge}. \tag{29}$$

3. Numerical results and discussion

Heat transfer to swirling flow of Bingham fluids along a rotating disk is modeled here. The normalized velocity and temperature profiles are computed from the equations (12)-(15), (18) and (19) by means of MATLAB routine bvp4c based on collocation formula. Following

Ahmedpour and Sadeghy [18], numerical integrations are carried out at $r^{\star}=1$, that is, at the rim of the disk for certain range of embedded parameters which include Eckert number Ec, Prandtl number Pr, Bingham number Bn and wall suction parameter A. Table 1 clearly shows good correlation of present results with those found by Ariel [7] and Turkyilmazoglu [14] in Newtonian fluid case with $A=0$. Table 2 displays the numerical results of wall skin friction $r^{\star}C_f$ at different values of Bn. Since apparent viscosity in the present problem is given by the factor $(1+Bn/\wedge)$ so we predict that skin friction coefficient should elevate as parameter Bn enlarges. Physically a growth in Bn implies an elevation in fluid yield stress (τ_y) which in turn results in higher resisting torque at the disk surface. In Table 3, local Nusselt number data is presented by varying the parameters $Bn,$ Pr and Ec. Note that by increasing fluid yield stress (τ_y), heat transfer through the disk deteriorates significantly. As Prandtl number enlarges, the relative importance of momentum diffusion increases due to which local Nusselt number enlarges. Furthermore, it is predicted that by increasing the intensity of viscous dissipation the rate of heat transfer from the solid surface should decrease.

The behavior of Bingham number Bn on all three velocities (u,v,w) and temperature profile θ is portrayed through Figs. 1a-1d at a specific parameter value $A=1$. Fig. 1a depicts that radially outward flow caused by centrifugal force decelerates throughout the boundary layer by increasing fluid yield stress. Maximum radial velocity is attained at a higher axial distance as parameter Bn enlarges. Fig. 1b displays the azimuthal velocity curves, represented by $G(\zeta)$, for various values of Bn. It is clear that circumferential velocity grows and boundary layer expands where fluid yield stress is enhanced. The reduction in radial fluid motion upon increasing Bn (as clarified in Fig. 1a) must be compensated by a decrease in downward axial velocity (see Fig. 1c). In other words, the pumping efficiency of the disk, that depends on absolute value of $H(\infty)$, is much reduced in the presence of yield stress. Physically the amount of fluid sucked from a region of lower temperature to a region of higher temperature decreases with increasing Bn. As a consequence, thermal boundary layer appears to expand upon increasing fluid yield stress (see Fig. 1d). Temperature curves become thick as Bn becomes large signaling a reduction in wall temperature gradient.

In Figs. 2a-2d, velocity and temperature curves as functions of dimensionless axial coordinate ζ are plotted for a variety of wall suction parameters. In existence of wall suction, radial velocity is substantially diminished compared with the same without any suction velocity (see Fig. 2a). The permeable nature of the disk also gives opposition to the induced azimuthal flow near the disk as clear from Fig. 2b. Dissimilar to the effect of Bingham number Bn, the volume of fluid drawn in the axial direction grows as wall suction becomes strong. It was shown by Turkyilmazoglu and Senel [8], via asymptotic expressions, that the axial velocity component becomes constant when sufficiently large suction velocity is imposed. The same tendency appears here since profile of H transforms into a straight line as parameter A increases. Consequently, thermal boundary layer suppresses with increasing A and magnitude of this decrease in θ becomes zero for sufficiently large values of A. In case of strong suction with negligible viscous dissipation, Eq. (18) can be directly integrated to give

$$\theta(\zeta)\sim \exp(-PrA\zeta). \quad (39)$$

Figs. 3a and 3b demonstrate the behaviors of Prandtl numberPr and Eckert number Ec on temperature profile respectively. In Fig. 3a, the thermal boundary layer suppress by increasing Pr. This is because the importance of thermal diffusion compared to momentum diffusion reduces with increasing Pr. Also, temperature profile becomes steeper when higher Pr is considered. This signals a growth in the magnitude of local Nusselt number. Eckert number measures the viscous dissipation effect which is heat generation induced in fluid flow as a result of friction. Large Eckert number ($Ec > 1$) can only be considered in special situations where fluid under consideration is either highly viscous or it flows with large velocity. By increasing Eckert number Ec, heat generation due to fluid friction enhances at a given temperature gradient. This in turn leads to thicker temperature profiles as anticipated.

Figs. 4a-4c display the wall skin friction $r^{\star}C_f$, local Nusselt number Nu and dimensionless volumetric flow rate $-H(\infty)$ as functions of Bingham number Bn. Computations are made at several values of wall suction parameter A. Eq. (21) shows that $r^{\star}C_f$ has a direct relation with Bingham number Bn. It is further clarified via Figs. 1a and 1b that wall velocity gradients $F'(0)$ and $G'(0)$ are decreasing functions of Bn. Due to these reasons, a decreasing trend in skin friction coefficient becomes apparent when Bn is incremented. Although, local Nusselt number is marginally influenced by Bingham number but it is significantly enhanced as wall suction gets strong. Fig. 4c shows that far field axial flow accelerates upon increasing wall suction parameter A. It should be noted that variation in $H(\infty)$ with Bn becomes smaller as parameter A gradually increases. Eventually, the graph of $H(\infty)$ versus Bn becomes a straight line in case of strong wall suction.

Entropy generation number N_G is a useful tool to predict spatial variation in entropy production across the boundary layer. Figs. 5a-5d plot the behaviors of different parameters on N_G. It appears that entropy production rate is maximum at the disk and it gradually decreases with increasing axial distance. A cross-over in N_G profiles is apparent in Fig. 5a illustrating that entropy generation decreases near the disk and increases near the edge of boundary layer when fluid's yield stress is enhanced. Fig. 5b elucidates that the impact of Prandtl number is to enhance the entropy production throughout the boundary layer. According to Fig.5c, the entropy generation rate is much enhanced when viscous dissipation effect is present. Fig. 5d depicts that higher the fluid yield stress, greater is the entropy production within the von-Kármán's boundary layer.

Table 1: Comparison with the numerical results obtained by Turkyilmazoglu [14] and Ariel [7] and when $Bn = A = Ec = 0$ and $Pr = 1$.

	Turkyilmazoglu [14]	Ariel [7]	Present
$F'(0)$	0.5102326	0.5102326191	0.510233
$G'(0)$	-0.6159220	0.6159220144	-0.615922
$H(\infty)$	-0.8844741	0.8844741002	-0.884472
$-\theta'(0)$	0.3962475	---------	0.396248

Table 2: Effect of Bingham number Bn on skin friction coefficient $r^{\star}C_f$ when $r^{*} = 1, Re = 2950$ and $A = 1$.

Bn	Pr	Ec	$F'(0)$	$G'(0)$	$r^{\star}C_f$
0	5	0.2	0.38956	-1.17522	0.02279
10	5	0.2	0.32344	-1.13896	0.02519
20	5	0.2	0.27708	-1.11538	0.02794

30	5	0.2	0.24208	-1.09859	0.03088
50	5	0.2	0.19274	-1.07631	0.03708

Table 3: Effect of Bingham number Bn, Prandtl number Pr and Eckert number Ec on local Nusselt number $-\theta'(0)$ when $r^* = 1, Re = 2950$ and $A = 1$.

Bn	Pr	Ec	$\theta'(0)$
0	5	0.2	-4.47919
10	5	0.2	-4.31126
20	5	0.2	-4.13891
30	5	0.2	-3.96382
50	5	0.2	-3.60851
10	2	0.2	-1.77831
10	3	0.2	-2.62405
10	5	0.2	-4.31126
10	7	0.2	-5.99953
10	5	0	-5.06572
10	5	0.2	-4.31126
10	5	0.4	-3.55681
10	5	0.6	-2.80235

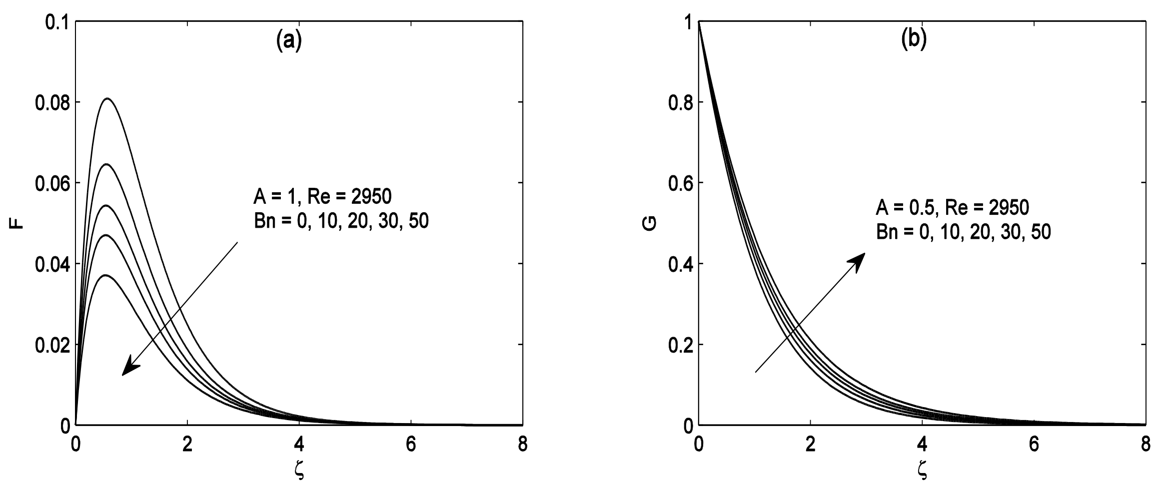

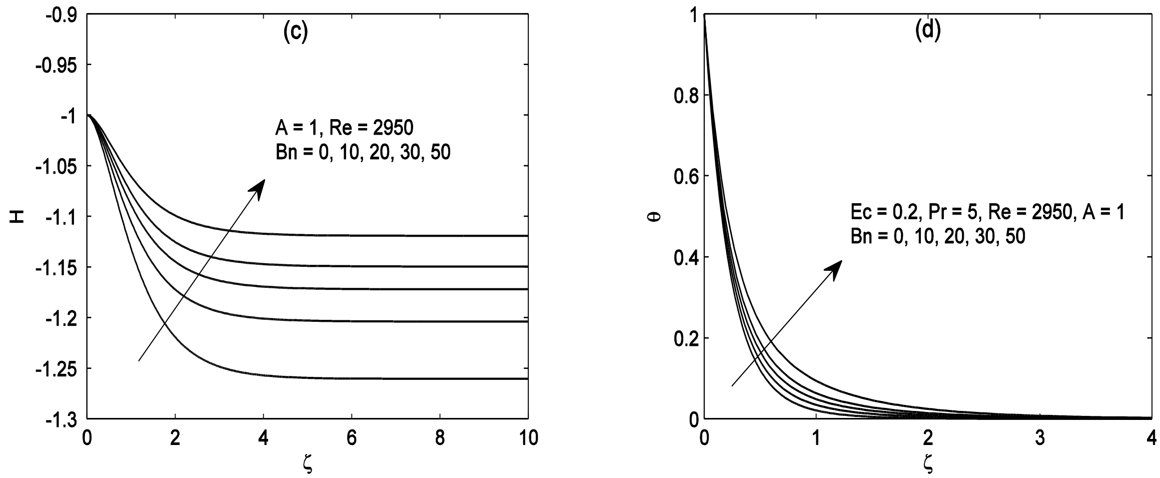

Fig. 1: Variation in normalized velocity components (F, G, H) and temperature (θ) with ζ at different values of Bingham number Bn.

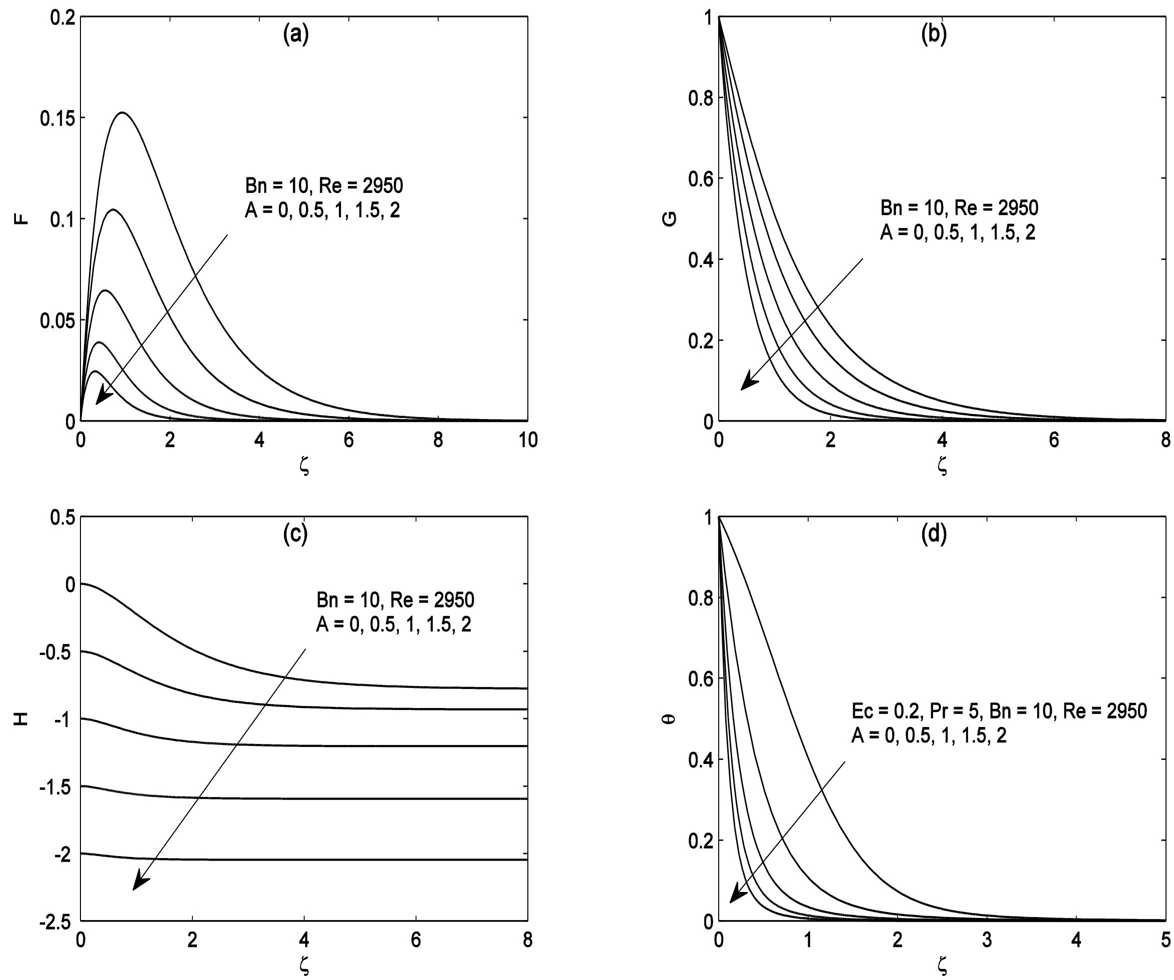

Fig. 2: Variation in normalized velocity components (F, G, H) and temperature (θ) with ζ for various values of wall suction parameter A.

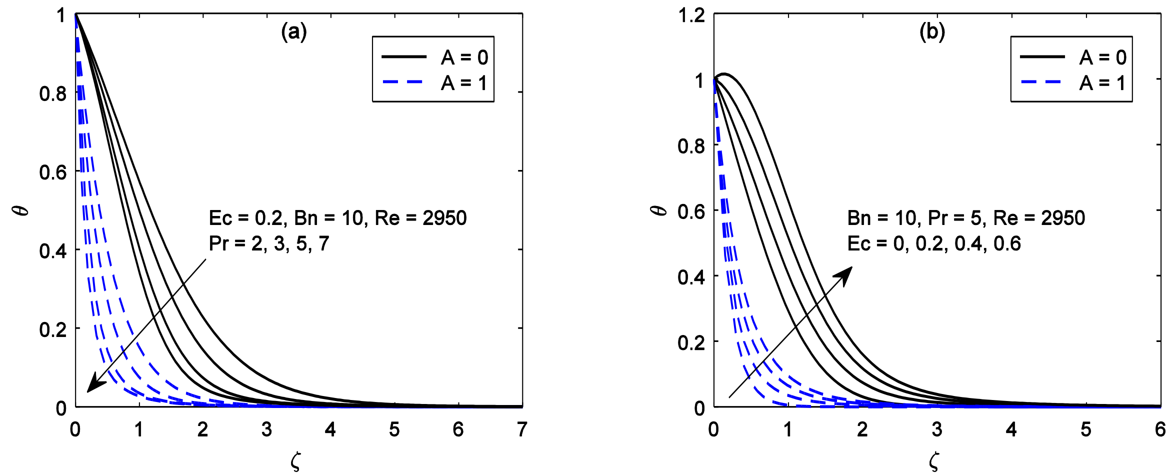

Fig. 3: Variation in temperature (θ) with ζ for different values of (a) Prandtl number Pr and (b) Eckert number (Ec).

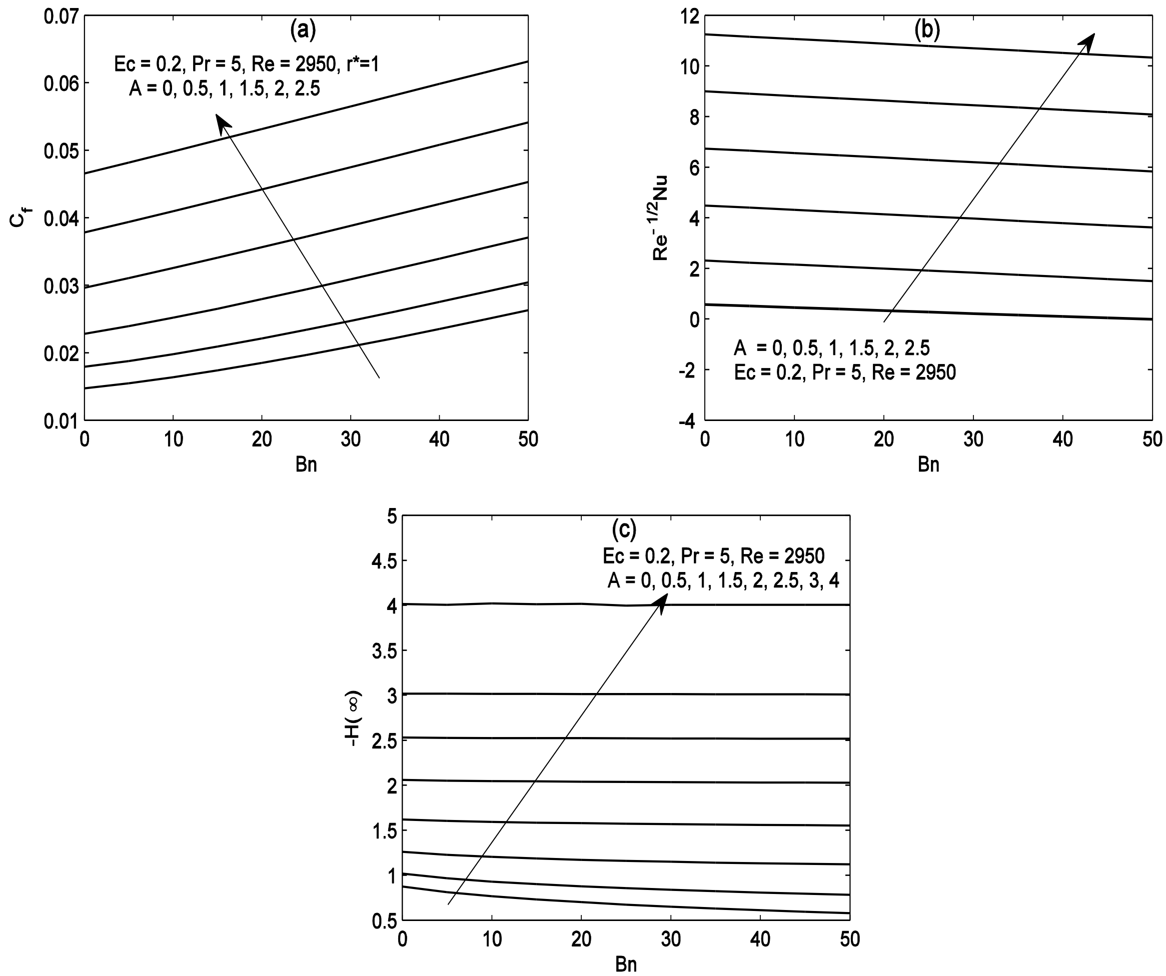

Fig. 4: Effect of Bingham number Bn and suction parameter A on (a) skin friction coefficient C_f, (b) local Nusselt number $Re^{-1/2}Nu$ and (c) dimensionless volumetric flow rate $-H(\infty)$.

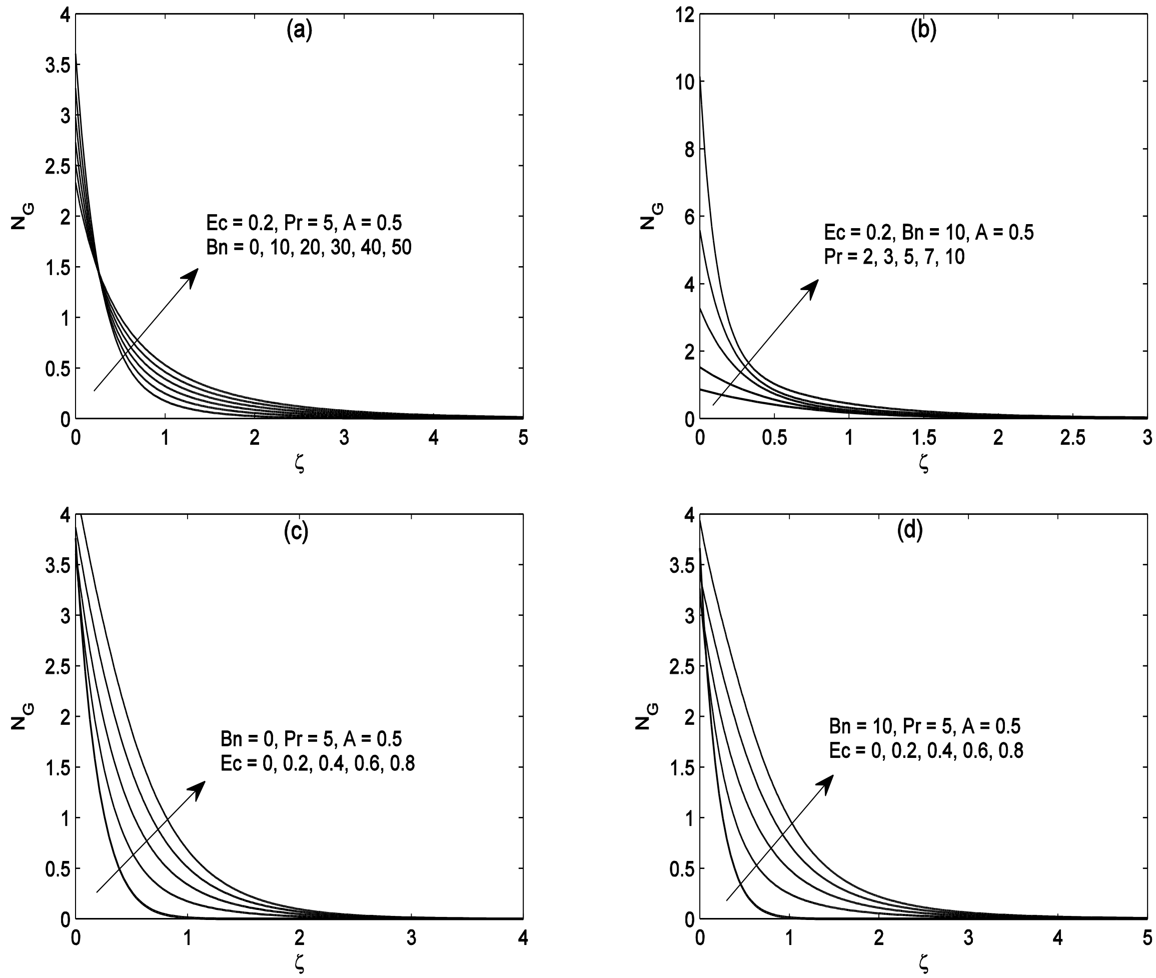

Fig. 5: Variation in entropy generation number N_G with ζ for various values of embedded parameters when $\alpha = 0.5$.

4. Concluding remarks

An analysis is carried out for heat transfer in von-Kármán flow of Bingham fluid subject to wall suction. A similarity solution is achieved that enabled us to discover the role of yield stress on heat transfer and entropy generation rate. On the basis of present work, following conclusions are drawn:

i. The retarding effect of fluid suction on the radial and azimuthal velocities is apparent from the numerical results.
ii. Axial velocity profile becomes constant as the wall suction effect enlarges. Furthermore, there is no variation in entrainment velocity $H(\infty)$ with Bingham number Bn in case of strong wall suction.
iii. Inclusion of wall suction phenomenon leads to an enhancement in the amount of cold fluid that is drawn towards the disk. This results in the thinning of thermal boundary layer and growth in wall heat transfer rate.
iv. The variation in solution profiles with increasing Bingham number reduces in magnitude when fluid is sucked at a higher velocity.

v. Heat penetration depth grows upon increasing fluid yield stress. This effect accompanies with lower heat transfer rate from solid surface.
vi. Entropy generation rate decreases monotonically with increasing vertical distance and asymptotes to zero value.
vii. The presence of yield stress has led to a growth in entropy generation rate within the boundary layer.

References

1. T. Von Kármán, Über laminare und turbulente Reibung, Zeitschrift fur Angew. Math. Mech. ZAMM 1 (1921) 233-252.
2. W. G. Cochran, The flow due to a rotating disk, Proceedings of the Cambridge Philosophical Society 30 (1934) 365–375.
3. G. K. Batchelor, Note on the class of solutions of the Navier–Stokes equations representing steady non-rotationally symmetric flow, Quart. J. Appl. Math. 4 (1951) 29-41.
4. U. T. Bödewadt, Die Drehströmungüberfestem Grund, Z. angew Math. Mech. 20 (1940) 241-252.
5. J. A. D. Ackroyd, On the steady flow produced by a rotating disk with either surface suction or injection, Journal of Engineering Mathematics 12 (1978) 207–220.
6. K. Millsaps and K. Pohlhausen, Heat transfer by laminar flow from a rotating disk, J. Aeronaut. Sci. 19 (1952) 120–126.
7. P. D. Ariel, On computation of MHD flow near a rotating disk, Z. Angew. Math. Mech. 82 (2002) 235-246.
8. A. Arikoglu and I. Ozkol, On the MHD and slip flow over a rotating disk with heat transfer, Int. J. Numer. Meth. Heat & Fluid Flow 16 (2006) 172-184.
9. M. Turkyilmazoglu and P. Senel, Heat and mass transfer of the flow due to a rotatingrough and porous disk, Int. J. Therm. Sci. 63 (2013) 146-158.
10. M. Turkyilmazoglu, Nanofluid flow and heat transfer due to a rotating disk. Comput. & Fluids 94 (2014) 139-146.
11. M. M. Rashidi, S. A. M. Pour, T. Hayat and S. Obaidat, Analytic approximate solutions for steady flow over a rotating disk in porous medium with heat transfer by homotopy analysis method, Comput. & Fluids 54 (2012) 1-9.
12. M. Mustafa, J. A. Khan, T. Hayat and A. Alsaedi, Numerical solutions for radiative heat transfer in ferrofluid flow due to a rotating disk: Tiwari and Das model, Int. J. Nonlinear Sci. Numer. Simul. 19 (2018); doi**:** https://doi.org/10.1515/ijnsns-2015-0196.
13. M. Mustafa, I. Pop, K. Naganthran and R. Nazar, Entropy generation analysis for radiative heat transfer to Bödewadt slip flow subject to strong wall suction, Eur. J. Mech. B/Fluids 72 (2018) 179-188.
14. M. Turkyilmazoglu, Fluid flow and heat transfer over a rotating and vertically moving disk, Phys. Fluids 30 (2018) doi: 10.1063/1.5037460.
15. A. Aziz, A. Alsaedi, T. Muhammad and T. Hayat, Numerical study for heat generation/absorption in flow of nanofluid by a rotating disk, Res. Phys. 8 (2018) 785 792.
16. A. Mehmood, M. Usman and B. Weigand, Heat and mass transfer phenomena due to a rotating non-isothermal wavy disk, Int. J. Heat & Mass Transf. 129 (2019) 96-102.

17. H. I. Andersson, E. de Korte and R. Meland, Flow of a power-law fluid over a rotating disk revisited, Fluid Dynam. Res. 28 (2001) 75-88.
18. A. Ahmadpour and K. Sadeghy, Swirling flow of Bingham fluids above a rotating disk: An exact solution, J. Non-Newtonian Fluid Mech. 197 (2013) 41-47.
19. A. Guha and S. Sengupta, Analysis of von Kármán's swirling flow on a rotating disc in Bingham fluids, Phys. Fluids 28 (2016) Article ID 013601, doi: https://doi.org/10.1063/1.4937590.
20. P. T. Griffiths, Flow of a generalised Newtonian fluid due to a rotating disk, J. Non-Newtonian Fluid Mech. 221 (2015) 9-17.
21. C. Ming, L. Zheng, X. Zhang, F. Liu and V. Anh, Flow and heat transfer of power-law fluid over a rotating disk with generalized diffusion, Int. Commun. Heat & Mass Transf. 79 (2016) 81-88.
22. S. Xun, J. Zhao, L. Zheng, X. Chen and X. Zhang, Flow and heat transfer of Ostwald-de Waele fluid over a variable thickness rotating disk with index decreasing, Int. J. Heat & Mass Transf. 103 (2016) 1214-1224.
23. M. Tabassum and M. Mustafa, A numerical treatment for partial slip flow and heat transfer of non-Newtonian Reiner-Rivlin fluid due to rotating disk, Int. J. Heat & Mass Transf. 123 (2018) 979-987.
24. M. M. Rashidi, S. Abelman and N. Freidooni Mehr, Entropy generation in steady MHD flow due to a rotating porous disk in a nanofluid, Int. J. Heat & Mass Transf. 62 (2013) 515-525.
25. M. Sheremet, I. Pop, H. F. Oztop and N. Abd-Hamdeh, Natural convection of nanofluid inside a wavy cavity with non-uniform heating: Entropy generation analysis, Int. J. Numer. Meth. Heat & Fluid Flow 27 (2017) 958-980.
26. T. Hayat, S. Qayyum, M. I. Khan and A. Alsaedi, Entropy generation in magnetohydrodynamic radiative flow due to rotating disk in presence of viscous dissipation and Joule heating, Phys. Fluids 30 (2018), Article ID 017101; doi: https://doi.org/10.1063/1.5009611.
27. M. Rahman and H. I. Andersson, On heat transfer in Bödewadt flow, Int. J. Heat & Mass Transf. 112 (2017) 1057-1061.